RFID-Based Localization of Mobile Robots Using the Received Signal Strength Indicator of Detected Tags

Christof Röhrig, *Member, IAENG,* Daniel Heß and Frank Künemund

Abstract—**Localization and tracking of mobile robots is an important issue for many industrial applications. The paper presents an inexpensive solution for indoor localization of mobile robots. Global localization is realized by interpreting the received signal strength indicator (RSSI) of RFID tags, which are integrated in the floor and detected by the reader. The paper presents two algorithms for fusing RFID signal strength measurements with odometry based on Kalman filtering. The paper presents experimental results with a Mecanum based omnidirectional mobile robot on a NaviFloor® installation, which includes passive HF RFID tags. The experiments show that the proposed algorithms provide a better performance compared to the same algorithms which consider the detection of the tags only.**

Index Terms—**RFID, RSSI, Mobile Robot, Localization, Pose Estimation, Constrained Kalman Filter**

Fig. 1. Floor installed RFID tags for localization of mobile robots

I. INTRODUCTION

INEXPENSIVE global localization of mobile robots is an important issue for many industrial applications and object of current research activities. Global localization is the process of estimating position and heading (pose) of a mobile robot in a cartesian space, without knowledge of the initial pose of the robot. A possible solution for global localization is the usage of auto-ID technology as artificial landmarks. Kiva Systems (now Amazon Robotics) uses 2D bar codes on the floor, which can be detected with a camera by the robots [1]. These bar codes specify the pathways and guarantee accurate localization. Drawbacks of this solution are the risk of polluting the bar codes and the need for predefined pathways, which restrict the movements of the robots.

Another possible solution for global localization is the usage of RFID technology as artificial landmarks. Passive RFID technology is often used in logistics and warehouse management for object identification and tracking. Typically the field of application is defined by the detection range of the RFID tags, which depends on the operation frequency. Usually LF or HF technology is used for self-localization of mobile systems (reader localization) and UHF technology is used for object identification in logistics applications [2] and service robotics [3].

The basic idea of using passive RFID tags as artificial landmarks for self-localization of mobile systems is not new. LF RFID tags are used to mark a predefined pathway for

navigation of Automated Guided Vehicles (AGVs) in industry since more than two decades [4].

A known disadvantage of using LF RFID tags for vehicle navigation is the speed limitation of the vehicles caused by the low data transfer rate of LF tags. Also LF tags are comparatively expensive and the ground must be prepared with holes for these tags [5]. Owing to the cost of installation and material, the tags are installed on the pathway of the vehicles only.

An inexpensive and much more flexible option is the usage of a grid of floor installed standard HF RFID tags. This allows free navigation of vehicles without the need of predefined pathways. The cost of a passive tag is less than $0.2\,€$. A commercially available product, which employs passive HF RFID tags in a floor is the NaviFloor® manufactured by Future-Shape. Technical details of the NaviFloor® can be found in Sec. V-A. Fig. 1 shows three omnidirectional mobile robots in our lab together with the NaviFloor® installation. The RFID tags illustrated in the picture are embedded in the floor and are not visible in reality.

The main contribution of this paper is the extension of the localization algorithms we have developed in [6] and [7], so that they fuse the RSSI from RFID readings with odometry. The proposed algorithms require a RFID reader with the capability of measuring the RSSI received from detected RFID tags. Our experimental results show that the evaluation of the received signal strength increases the accuracy of the proposed algorithms.

The rest of the paper is organized as follows: In Sec. II the localization problem using floor installed RFID tags is defined. Sec. III presents related work. The proposed localization algorithms are developed in Sec. IV. In Sec. V the experimental setup including NaviFloor® and RFID reader

is described. Experimental results are presented in Sec. VII. Finally, the conclusions are given in Sec. VIII. This paper extends the work presented in [8].

II. Problem Formulation

We consider the problem of global localizing a robot in a known environment. In this context, global localization means that the initial pose of the robot is not known a priori. The robot is equipped with a RFID reader and moves over a floor with n RFID tags. The position of the tags is known a priori. The robot moves in 2D space, the pose of the robot (position and heading) in the world frame is defined as $x = (x, y, \theta)^T$ in the configuration space (C-space) $\mathcal{C}$, which is a subset of $\mathbb{R}^3$. $\mathcal{C} = \mathbb{R}^2 \times \mathcal{S}^1$ takes into account that $\theta \pm 2\pi$ yields to equivalent headings ($\theta \in [0, 2\pi)$). If a tag $T_i \in \{T_1, \ldots, T_n\}$ with position $t_i = (x_i, y_i)^T$ (defined in the world frame) is in range of the reader antenna, it is detected by the robot. The area where a tag can be detected by the reader is the detection area $\mathcal{A}$. The reader receives a signal strength, when it detects a RFID tag. The received signals strength indicator (RSSI) becomes larger, when the overlap of the reader antenna and the tag antenna increases. We assume that the distance of the reader antenna to the ground is always constant. Furthermore, it is assumed that the RSSI is measured in discrete increments $j \in \{0, \ldots, m\}$, where 0 is the lowest signal strength and m is the highest value. For every possible RSSI increment j an area $\mathcal{A}_j$ can be described, where this value can be received. The detection areas may have an overlap. The detection areas can be described in the antenna frame, which is in a fixed position in the robot frame. Size and shape of $\mathcal{A}_j$ depend on the reader antenna, the tag type and the distance between them and is the same for all tags. The position of a tag in the antenna frame $z_i = (^Ax_i, ^Ay_i)^T$ can be described by

$$z_i = h(x, t_i), \tag{1}$$

where x is the pose of the robot and t_i is the position of the tag T_i, both defined in the world frame.
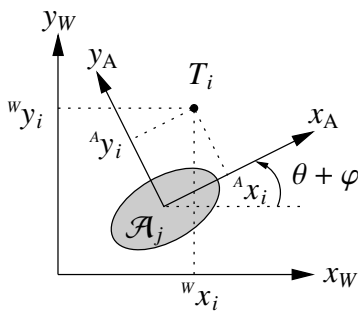

Fig. 2. Position of RFID tag in world frame $(^Wx_i, ^Wy_i)^T$ and in antenna frame $(^Ax_i, ^Ay_i)^T$. The detection area $\mathcal{A}_j$ is marked in gray.

Fig. 2 shows the position of a RFID tag in the world frame and in the antenna frame. The rotation angle between the antenna frame and the world frame depends on the heading of the robot (θ) and the constant alignment of the antenna (φ) with respect to the robot frame.

$h(\cdot)$ can be defined by a homogeneous transformation in 2D:

$$\tilde{z} = {}^A T_W(x) \cdot \tilde{t}, \tag{2}$$

where the transformation matrix

$$ {}^A T_W(x) = {}^A T_R \cdot {}^R T_W(x) $$

consists of the constant transformation from robot frame into antenna frame ${}^A T_R = f(x_A, y_A, \varphi)$ and the transformation from world frame into robot frame ${}^R T_W$, which depends on the pose of the robot ${}^R T_W = f(x)$ with $x = (x, y, \theta)^T$:

$$ {}^R T_W = \begin{pmatrix} \cos\theta & \sin\theta & -x\cos\theta - y\sin\theta \\ -\sin\theta & \cos\theta & x\sin\theta - y\cos\theta \\ 0 & 0 & 1 \end{pmatrix}, $$

$$ {}^A T_R = \begin{pmatrix} \cos\varphi & \sin\varphi & -x_A\cos\varphi - y_A\sin\varphi \\ -\sin\varphi & \cos\varphi & x_A\sin\varphi - y_A\cos\varphi \\ 0 & 0 & 1 \end{pmatrix}, $$

$\tilde{z}$ and $\tilde{t}$ are homogeneous coordinates in 2D $(x, y, 1)^T$.

When detecting tag T_i with RSSI j, the position $z_i = (^Ax, ^Ay)^T$ must be inside the detection area $\mathcal{A}_j$:

$$p(z_i \in \mathcal{A}_j | T_i, \text{RSSI} = j) = 1 \tag{3}$$

RSSI readings j outside of $\mathcal{A}_j$ do not arise, owing to the short range of HF RFID technology. Therefore, the RSSI reading j from tag T_i can be treated as detection that $z_i \in \mathcal{A}_j$.

Bayesian filtering is a solution for estimating the pose of a robot using RFID readings and odometry. Aim of the pose estimation using RFID readings is to obtain the probability density $p(x_k | T_i, \text{RSSI} = j, x_{k-1}, u_k) = p(x_k | z_i \in \mathcal{A}_j, x_{k-1}, u_k)$, where u_k is the odometry of the robot obtained from wheel encoders. This can be achieved by applying a Bayesian filter:

$$p(x_k | z_i \in \mathcal{A}_j, x_{k-1}, u_k) = \frac{p(z_i \in \mathcal{A}_j | x_k) p(x_k | x_{k-1}, u_k)}{p(z_i \in \mathcal{A}_j)} \tag{4}$$

where $p(z_i \in \mathcal{A}_j | x_k)$ is the probability of measuring T_i with RSSI j at the pose x in time step k and $p(x_k | x_{k-1}, u_k)$ is the motion model of the mobile robot. Due to the highly non-Gaussian probability distribution of RFID tag readings, usually Particle Filters (PF) are used for this purpose. In a PF, the probability density of the pose estimate is approximated by a set of particles. Every particle in the set represents a weighted hypothesis of the pose x. This enables the filter to handle non-Gaussian and multimodal distributions. After a tag is detected, every particle in the set is distributed through function (1) and weighted with probability (3). Main drawback of the PF is the computational expense associated with it, because only large particle counts lead to good pose estimates. Thus, there is some effort to replace the PF with methods based on Kalman filtering.

A RFID measurement can be interpreted as a *quantized measurement* of a position, which may depend on the headings of the robot. The quantization depends on the size of $\mathcal{A}_j$ and can be modeled by quantization noise. This interpretation leads to a localization algorithm, which is based on Quantized Kalman filtering [6]. In order to reduce the number of tags needed in the grid, the size of the grid and therefore the detection area has to be relatively large. If the detection area compared to the grid size is small, the chance of detecting a tag while traveling over the grid decreases, which reduces the localization accuracy. Main drawback of Quantized Kalman filtering is the large quantization noise for large detection areas, which leads to low estimation accuracy.

A different interpretation of a RFID measurement T_i is that the pose of the robot falls in a *constrained region* in

the C-space C. This detection region $\mathcal{R}_i \subset C$ is defined by the position of the tag $\boldsymbol{t}_i = (x, y)^{\mathrm{T}}$ in the world frame, the placement of the antenna with respect to the robot frame $^{\mathrm{R}}\boldsymbol{T}_{\mathrm{W}}$ and the shape of the detection area $\mathcal{A}_j$ in the antenna frame. The detection region $\mathcal{R}_i$ can be interpreted as an extension of the 2D detection area $\mathcal{A}_j$ to the 3D C-space of the robot. This means that the position of the robot falls in a bounded area, which depends on the heading of the robot. This interpretation leads to a localization algorithm, which is based on Constrained Kalman filtering [7]. In this paper both algorithms are extended to support RSSI measurements.

III. Related Works

In order to allow free navigation of mobile robots, some research on RFID localization using a grid of floor-installed RFID tags has been done. Kodaka et al. apply a PF for pose estimation of a mobile robot using floor based RFID tag and odometry [9]. Mi and Takahashi localize an omnidirectional vehicle using a RFID system with multiple readers [10]. They compare configurations with different numbers of readers and tag densities [11]. They develop a likelihood function of tag detection which is suitable for localization using PF. As mentioned above, main drawback of the PF is the computational expense associated with it. Thus, there is some effort to replace the PF with methods based on Kalman filtering. Choi et al. propose the fusion of ultrasonic sensors, odometry and readings of HF RFID tags, which are integrated in the floor [12]. This localization algorithm is based on Kalman filtering but needs additional sensors and mapping of the environment. Lee et al. have developed a Gaussian measurement model for UHF RFID tags embedded in the floor, which is suitable for Kalman filtering [13]. Its application in a Kalman filter has less computational expense but provides not the same localization accuracy as a PF.

There is also some research on UHF tags at walls or ceilings for self-localization of mobile robots. DiGiampaolo and Martinelli have developed a Quantized Extended Kalman Filter algorithm for localization on mobile robots using UHF RFID tags at the ceiling [14]. Boccadoro et. al. propose a Constrained Kalman filter for global localization of mobile robots using UHF RFID technology and odometry [15]. In that research, the tags are placed at the walls in an indoor environment. As in this paper, their proposed algorithms are based on Constraint and Quantized Kalman filtering. Since wall placed UHF tags provide a different detection behavior than floor placed HF tags, their localization algorithms are different to the algorithms proposed in this paper. Levratti et. al. present a localization algorithm for robotic lawnmowers based on the Constrained Kalman filter proposed in [15]. It merges odometry with UHF RFID tags, which are placed at the borders of the working area [16].

The usage of HF tags in the floor for self-localization has some advantages over usage of long range UHF technology at the walls or the ceiling. Usually the detection area is smaller and therefore the localization accuracy is better compared to long range UHF technology. HF RFID technology behaves different from long range UHF RFID technology, that is investigated in the research mentioned above, and therefore needs different modeling. In particular, floor placed HF RFID tags have a nearly binary detection characteristic, where the

detection area depends mainly on size and shape of the reader's antenna.

There is some research on technical aspects of self-localization using HF RFID tagged floor like antenna design [5], [17], antenna placement on the vehicle, [18], [19], tag placement on the floor [20], and optimal detection range of the reader [21].

IV. Proposed Localization Algorithms

This section describes the pose estimation in three different types of Bayesian filters. A Bayesian filter for robot localization needs a motion model of the robot and a sensor model of its measurements. The proposed algorithms are independent of the motion model. For experimental evaluation, we use an omnidirectional robot with Mecanum wheels. In this section, the sensor model of RFID readings and the proposed algorithm for measurement update of the Bayesian filters are described. As mentioned before, usually PFs are deployed in RFID localization algorithms, because of the highly nonlinear and quantized measurements by the RFID reader. A PF will be used as benchmark for our proposed localization algorithms based on Kalman filtering.

A. Quantized Kalman Filtering

In this section, the Quantized Kalman filter we have proposed in [6] and [7] is extended to RSSI measurements. The detection of a tag can be considered as a quantized measurement of a position. The center of the detection area $\mathcal{A}_j$ defines the position measurement in the antenna frame. The size of $\mathcal{A}_j$ is a measure of the uncertainty in the measurement and can be modeled as quantization noise. After detecting the tag T_i with RSSI j, the predicted measurement is defined by $\hat{\boldsymbol{z}}_i = \boldsymbol{h}(\hat{\boldsymbol{x}}_k, \boldsymbol{t}_i, \boldsymbol{0})$.

The *Gaussian-Fit Algorithm* proposed by Curry [22, p. 23–25] is applied to nonlinear Kalman filtering. The first and second moment of $p(z_i|z_i \in \mathcal{A}_j)$ are needed in the measurement update of a nonlinear KF. For notational convenience let

$$\boldsymbol{\mu}_j = \mathrm{E}(z_i|z_i \in \mathcal{A}_j), \quad \boldsymbol{\Sigma}_j = \mathrm{cov}(z_i|z_i \in \mathcal{A}_j).$$

Mean $\boldsymbol{\mu}_j$ and covariance $\boldsymbol{\Sigma}_j$ of the detection area $\mathcal{A}_j$ can be calculated in advance using numerical integration (see [6]). These calculations are necessary for every possible RSSI measurement j. Beside this quantized nature of RFID measurements there are additional sources of uncertainty:

- Communication delay between the RFID reader and the tag: This delay is caused by the limited data rate of the air interface and the collision avoidance procedure for multi tag readings.
- Communication delay between the control system and the RFID reader: This delay is caused by the processing time of the reader and the limited data rate on the interface to the reader.
- Variations in tag placement: Due to production tolerances and manual placement, the position of the RFID tags may differ from the regular grid.

The uncertainty in the tag placement can be treated as Gaussian noise. The communication delays causes additional noise that depends on the speed of the robot. These uncertainties

can be modeled with a random variable v_k. It is assumed that $v_k \sim \mathcal{N}(\mathbf{0}, \mathbf{R}_k)$.

Before the measurement update is performed, the innovation of the measurement T_i with RSSI j is checked. If $\hat{z}_i = h(\hat{x}_k, t_i, \mathbf{0}) \in \mathcal{A}_j$, the detection of T_i is predicted and the innovation is zero (the detection of T_i gives no additional information). Thus, no measurement update is performed. The measurement update is performed only, if $\hat{z}_i \notin \mathcal{A}_j$. The described algorithm can be applied to the measurement update of any nonlinear Kalman filter. The application of the standard EKF algorithm leads to:

$$K_k = P_k H_k^{\mathrm{T}} \left(H_k P_k H_k^{\mathrm{T}} + V_k (R_k + \Sigma_j) V_k^{\mathrm{T}} \right)^{-1} \quad (5)$$

$$\hat{x}_k^+ = \hat{x}_k + K_k \left(\mu_j - h(\hat{x}_k, t_i, \mathbf{0}) \right) \quad (6)$$

$$P_k^+ = (I - K_k H_k) P_k \quad (7)$$

where K_k is the Kalman gain, $\hat{x}_k^+$ and P_k^+ are the estimated pose and its covariance after the RFID measurement update, $H_k = \frac{\partial h}{\partial x}(\hat{x}_k, t_i, \mathbf{0})$ and $V_k = \frac{\partial h}{\partial v}(\hat{x}_k, t_i, \mathbf{0})$.

B. Constrained Kalman Filter

In this section, the Constrained Kalman filter we have developed in [7] is extended to handle RSSI measurements. A RFID measurement with RSSI j gives the information that a tag T_i with the position t_i is inside of the detection area $\mathcal{A}_j$ of the reader. Additional measurement noise caused by communication delays and tag misplacement due to production tolerances are modeled with the random variable v_k. It is assumed that $v_k \sim \mathcal{N}(\mathbf{0}, \mathbf{R}_k)$. With this additional uncertainty, the measurement function (1) can be extended:

$$z_i = h(x, t_i, v), \quad (8)$$

When the RFID tag T_i is detected with RSSI j, the position z_i must be inside the detection area $\mathcal{A}_j$. This implies, that the pose of the robot must be inside the detection region $x \in \mathcal{R}_{i,j}$, with $\mathcal{R}_{i,j} \subset C$. The detection region $\mathcal{R}_{i,j}$ is defined by the position of the tag $t_i = (x, y)^{\mathrm{T}}$ in the world frame, the placement of the antenna with respect to the robot frame and the shape of the detection area $\mathcal{A}_j$ in the antenna frame (see Sec. II). This information can be interpreted as a noisy nonlinear state inequality constraint [23].

In order to define the state constraints of the robot, we define a nonlinear function

$$d_{i,j} = g(z_i, j) \quad (9)$$

that describes the distance of the tag T_i to the border of $\mathcal{A}_j$, where

$$g(z_i, j) \begin{cases} \leq 0 & \text{if } z_i \in \mathcal{A}_j \\ > 0 & \text{else} \end{cases} \quad (10)$$

A nonlinear state inequality constraint can be transformed into a nonlinear state equality constraint [24], since two cases can occur:

1) The inequality is satisfied and so do not have to be taken into account.
2) The inequality is not satisfied. Then, the equality constraint has to be applied.

Owing to the uncertainty in RFID measurements, we treat the (soft) equality constraint as a noisy measurement:

$$g(z_i, j) = g(h(x, t_i, v), j) = 0 \quad (11)$$

1) If the inequality constraint (10) is satisfied, no measurement update of the Kalman filter is applied.
2) If a tag T_i is detected but $g(\hat{z}_i, j) > 0$, then we apply a measurement update $g(\hat{z}_i, j) = 0$ in every time step k until the constraint is satisfied.
3) If the tag is not longer detected, but the pose estimate persists in $\mathcal{R}_{i,j}$, which means that $g(h(\hat{x}_k, t_i, \mathbf{0}), j) < 0$, then we apply a measurement update $g(\hat{x}_k, j) = 0$ again in every time step k until the constraint is satisfied.

Every measurement update moves the pose estimate in direction of the border of $\mathcal{R}_{i,j}$. This algorithm is applicable for any RFID equipment, where the border of the detection area can be described by a nonlinear function (11). If more than one tag can be detected at a moment, the constraints of all detected tags have to be considered simultaneously. The described algorithm can be applied to any nonlinear Kalman filter, e.g. the well known Extended Kalman Filter (EKF).

The application of the proposed algorithm to the measurement update of an EKF leads to

$$K_k = P_k G_k^{\mathrm{T}} \left(G_k P_k G_k^{\mathrm{T}} + V_k R_k V_k^{\mathrm{T}} \right)^{-1}$$

$$\hat{x}_k^+ = \hat{x}_k - K_k \, g(h(\hat{x}_k, t_i, \mathbf{0}), j)$$

$$P_k^+ = (I - K_k G_k) P_k \quad (12)$$

where K_k is the Kalman gain, $\hat{x}_k^+$ and P_k^+ are the estimated pose and its covariance after the RFID measurement update, $G_k = \frac{\partial g}{\partial x}(\hat{x}_k, t_i, \mathbf{0})$, $V_k = \frac{\partial g}{\partial v}(\hat{x}_k, t_i, \mathbf{0})$ and R_k is the covariance matrix of the uncertainty $v_k \sim \mathcal{N}(\mathbf{0}, \mathbf{R}_k)$.
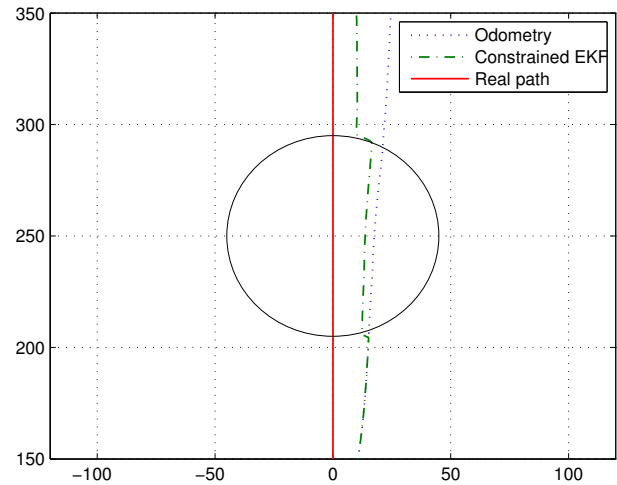

Fig. 3.   Visualization of Constrained EKF

Fig. 3 shows results from a simulation and demonstrates the working principal of the Constrained Kalman filtering. For simplification it is assumed that the reader antenna is mounted in the center of the vehicles frame ($^{\mathrm{A}}T_{\mathrm{V}} = I$). Furthermore, it is assumed that the RFID reader measures always the same RSSI value while detecting the tag. In the simulation, the detection area $\mathcal{A}_j$ is described by a circle with radius $r = 45\,\mathrm{mm}$. In this case, the detection region $\mathcal{R}_i$ of the tag T_i has a cylindric shape in the state space of the vehicle. The projection of $\mathcal{R}_i$ onto the 2D working area is a circle with radius r and center at t_i.

The vehicle moves from position (0, 0) in y direction with $\dot{y} = 100\,\mathrm{mm/s}$. The sample time for the motion update (odometry) is $T = 3\,\mathrm{ms}$, the update time of the RFID reader is

$T_{\text{RFID}} = 21$ ms. The pose estimated by odometry is corrupted by noise and is shown as blue curve. The real trajectory is shown in red, the estimate in green. A RFID tag T_1 is placed at $x_1 = 0$ mm, $y_1 = 250$ mm. After the tag T_1 is detected, the constraint $g(\boldsymbol{h}(\hat{\boldsymbol{x}}_k, \boldsymbol{t}_1, \boldsymbol{0}) \leq 0$ is checked. Since the constraint is not satisfied, a measurement update is applied, which moves the pose estimate to the border of $\mathcal{R}_1$. This update is repeated in every time step k until the constraint is satisfied. If the constraint is satisfied, while the vehicle is moving through the detection region, no measurement updates are applied. After the estimated pose leaves $\mathcal{R}_1$, measurement updates are applied in every time step k until the tag is not longer detected. This moves the estimated pose $\hat{\boldsymbol{x}}_k$ in direction of the border of $\mathcal{R}_1$ again. The correction of $\hat{\boldsymbol{x}}_k$ depends on its covariance matrix $\boldsymbol{P}_k$ and the shape of $\mathcal{A}$. Thus, there is a small remaining pose error in x direction.

C. Particle Filter

As mentioned before, usually PFs are deployed in RFID localization algorithms, because of the highly nonlinear and quantized measurements by the RFID reader. A PF will be used as benchmark for our proposed localization algorithms based on Kalman filtering.

In the motion update of a PF, all particles are sampled with a random generator and distributed through the motion model of the robot. The measurement update in a particle filter is straight forward (see also [9]). After the robot has detected a RFID tag, each particle $\boldsymbol{x}_k^n$ is distributed through the measurement function $z_i^n = \boldsymbol{h}(\boldsymbol{x}_k^n, \boldsymbol{t}_i, \boldsymbol{0})$ and then weighted with the associated probability $(w_n = p(T_i|\boldsymbol{z}_i^n))$, which depends on $\mathcal{A}_j$ and therefore on the detected RSSI. The measurement noise can be modeled with a normal distribution $\boldsymbol{v}_k \sim \mathcal{N}(\boldsymbol{0}, \boldsymbol{R}_k)$.

If no particle falls inside the detection area $(\sum w_n \approx 0)$, the particle set has to be reinitialized. In this case, the particles are uniformly distributed in the detection region $\mathcal{R}_i$. Otherwise, the particle set is normalized and resampled.

D. Global Localization

A Kalman filter has to be initialized with a rough initial pose estimate of the robot. Since a RFID reading provides no information about the heading of the robot, at least two different RFID tags have to be detected to initialize a Kalman filter. This initial procedure is a kind of map-matching between the initial local map of the robot processed by odometry and the global map including the positions of the tags. The heading can be estimated after detecting two different RFID tags (T_i, T_j):

$$\hat{\theta}_k = \theta_k^{\text{l}} + \text{atan2}(\Delta y, \Delta x) - \text{atan2}(\Delta y^{\text{l}}, \Delta x^{\text{l}}), \quad (13)$$

where θ_k^{l} is the local heading while detecting the second tag, $\Delta x = x_j - x_i$, $\Delta y = y_j - y_i$ are the distances between the detected tags and $\Delta y^{\text{l}}, \Delta x^{\text{l}}$ are the distances of the trajectory traveled in the local map. θ_k^{l} has to be considered, because an omnidirectional robot can move in any direction without changing its heading. The estimation of $\hat{\theta}_k$ is very rough, because $\Delta x \, \Delta y$ are quantized with the grid size of the RFID tags.

V. RFID Sensor Setup

A. NaviFloor®

The NaviFloor® is a glass fiber reinforcement in which passive HF RFID tags are embedded. The NaviFloor® underlay is shipped in rolls including a map of the RFID tags for simplification of the installation [25]. The NaviFloor® is specially developed for installation beneath artificial flooring. It is pressure-resistant up to 45 N/mm² and withstands even heavy indoor vehicles like fork lift trucks.

We have installed a NaviFloor® in our robotics lab. The RFID tags are installed in a grid of 25 cm. The whole installation includes nearly thousand RFID tags. The tags embedded in the NaviFloor® have a rectangular shape 45 mm × 45 mm. NXP chips I-CODE SLI are integrated in the tags. The tags are compliant to ISO 15693 and communicate in the 13.56 MHz HF band.

B. RFID Reader

The reader used in our experiments is a "KTS SRR1356 ShortRange HF Reader" with an external antenna with the rectangular shape 80 mm × 80 mm. We have mounted the reader at a distance of 15 mm to the floor. At this distance, the detection areas of the reader have circular shapes. The reader measures RSSI in 8 increments, all detection areas $\mathcal{A}_j$ can be modeled with a circular shape but a different radius r_j:

TABLE I
RADIUS OF DETECTION AREA DEPENDING ON MEASURED RSSI

RSSI	0	1	2	3	4	5	6	7
radius in mm	105	100	95	90	80	60	50	40

The RFID tags in the floor are placed in a regular grid of 250 mm. Thus, at most one RFID tag can be detected at any moment. The reader is mounted in the center of the robot frame $(^{\text{A}}\boldsymbol{T}_{\text{R}} = \boldsymbol{I})$. Thus, the heading of the robot has no impact on the reading region $\mathcal{R}_i$. In case of our experimental setup, the border of the detection area can be modeled

$$g(\boldsymbol{h}(\boldsymbol{x}_k, \boldsymbol{t}_i, \boldsymbol{v}_k)) = \sqrt{(x_k - x_i + v_x)^2 + (y_k - y_i + v_y)^2} - r_j \quad (14)$$

where x_i, y_i is the position of T_i in world frame, x_k, y_k is the position of the robot (center of the robot frame), r_j is the radius of the detection area $\mathcal{A}_j$ at RSSI j and $\boldsymbol{v}_k = (v_x, v_y)^{\text{T}}$ is the measurement noise. In oder to apply the measurement update $g(\boldsymbol{x}_k, \boldsymbol{v}_k)$ to an EKF its Jacobians are needed:

$$\boldsymbol{G}_k = \frac{\partial g}{\partial \boldsymbol{x}}(\hat{\boldsymbol{x}}_k, \boldsymbol{t}_i, \boldsymbol{0}) = \quad (15)$$

$$\left(\frac{x_k - x_i}{\sqrt{(x_k - x_i)^2 + (y_k - y_i)^2}} \quad \frac{y_k - y_i}{\sqrt{(x_k - x_i)^2 + (y_k - y_i)^2}} \quad 0 \right),$$

and

$$\boldsymbol{V}_{k,i} = \frac{\partial g_i}{\partial \boldsymbol{v}}(\hat{\boldsymbol{x}}_k, \boldsymbol{t}_i, \boldsymbol{0}) = \boldsymbol{G}_{k,i} \quad (16)$$

Mean and covariance of the detection areas $\mathcal{A}_j$ are needed for the Quantized Kalman filter. In case of a circular shape, $\boldsymbol{\mu}_j$ is the center of the circle in the antenna frame and

$$\boldsymbol{\Sigma}_j = \begin{pmatrix} \frac{r_j^2}{4} & 0 \\ 0 & \frac{r_j^2}{4} \end{pmatrix}$$

where r_j is the radius of $\mathcal{A}_j$.

VI. Motion Model for Mobile Robot with Mecanum Wheels

In this section, a motion model for omnidirectional vehicles with Mecanum wheels is derived, which is suitable for poses estimation using an Extended Kalman Filter (EKF). The motion model is based on experiments with our Mecanum driven omnidirectional vehicles and extends the work presented in [26]. An omnidirectional vehicle is able to move in any direction and rotate around its z-axis at the same time. The motion models found in literature are limited to mobile robots with two degrees of freedom. The motion model is based on odometry measurements obtained from wheel encoders. Odometry can be treated as controls, because most vehicle control systems control the movements of the vehicle in a closed position control loop based on odometry. In this case, the command values of the control loop correspond directly to odometry. The movements of the vehicle are corrupted by disturbances caused by mechanical inaccuracies such as uneven floor, wheel slippage and inaccuracies in the speed control of the wheels that lead to coupling errors. This disturbances will be treated as process noise.
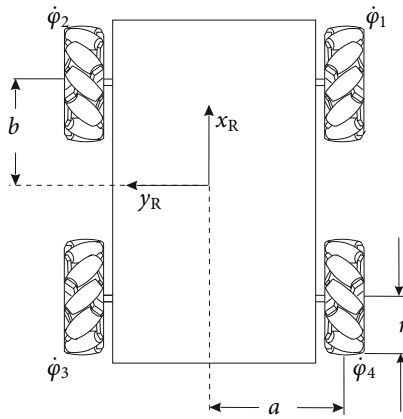

Fig. 4. Omnidirectional vehicle with Mecanum wheels

The vehicle is equipped with Mecanum wheels and electronic drives, which provide three degrees of freedom. The omnidirectional vehicle possesses four motor driven Mecanum wheels. The wheel configuration of the mobile system is shown in **Figure 4**. The velocities in the vehicle (robot) frame ($\dot{x}_R$, $\dot{y}_R$, $\dot{\theta}$) are a function of the four wheel velocities $\dot{\varphi}_1 \ldots \dot{\varphi}_4$:

$$\begin{pmatrix} \dot{x}_R \\ \dot{y}_R \\ \dot{\theta} \\ \dot{\varphi}_e \end{pmatrix} = J \begin{pmatrix} \dot{\varphi}_1 \\ \dot{\varphi}_2 \\ \dot{\varphi}_3 \\ \dot{\varphi}_4 \end{pmatrix}, \quad J = \frac{r}{4} \begin{pmatrix} 1 & 1 & 1 & 1 \\ -1 & 1 & -1 & 1 \\ \frac{1}{a+b} & \frac{-1}{a+b} & \frac{-1}{a+b} & \frac{1}{a+b} \\ \frac{4}{r} & \frac{4}{r} & -\frac{4}{r} & -\frac{4}{r} \end{pmatrix} \quad (17)$$

where r is the radius of the wheels, a and b are given by the dimension of the vehicle (see Figure 4). An angular error velocity $\dot{\varphi}_e \neq 0$ causes a coupling error of the wheels and thus additional wheel slippage. Eqn. (17) is used in the operating system of the vehicle to execute odometry. The inverse equation transforms velocities in vehicle frame into the wheel velocities:

$$\begin{pmatrix} \dot{\varphi}_1 \\ \dot{\varphi}_2 \\ \dot{\varphi}_3 \\ \dot{\varphi}_4 \end{pmatrix} = J^{-1} \begin{pmatrix} \dot{x}_R \\ \dot{y}_R \\ \dot{\theta} \\ \dot{\varphi}_e \end{pmatrix} \quad (18)$$

Eqn. (18) is used in the operating system of the vehicle to control the speeds in vehicle frame. The control variable $\dot{\varphi}_e$ can be used to force the coupling error φ_e to zero [27]. For more details about the kinematics of the vehicle refer to [28], [29].

Velocities in the vehicle frame can be transformed into the world frame, if the heading θ of the vehicle is known.

$$\dot{x}_R = R(\theta)\, \dot{x}_W, \quad \Rightarrow \quad \dot{x}_W = R^{-1}(\theta)\, \dot{x}_R \quad (19)$$

$$\text{with} \quad \dot{x}_W = \begin{pmatrix} \dot{x}_W \\ \dot{y}_W \\ \dot{\theta} \end{pmatrix}, \dot{x}_R = \begin{pmatrix} \dot{x}_R \\ \dot{y}_R \\ \dot{\theta} \end{pmatrix},$$

$$R(\theta) = \begin{pmatrix} \cos\theta & \sin\theta & 0 \\ -\sin\theta & \cos\theta & 0 \\ 0 & 0 & 1 \end{pmatrix}$$

Between two time steps of odometry it is assumed, that the omnidirectional vehicle moves on a straight line while it rotates from θ_{k-1} to θ_k at the same time (see **Figure 5**). To simplify calculations, this movement is divided into three independent movements. First a rotation $\Delta\theta/2$, than a translation (Δx, Δy) without rotation and finally again a rotation $\Delta\theta/2$.
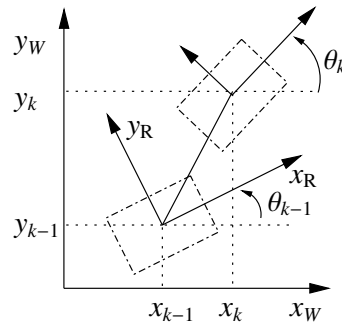

Fig. 5. Movement of an omnidirectional vehicle

The movements described in directions of the vehicle frame can be calculated with (17) as:

$$\begin{pmatrix} \Delta x_R \\ \Delta y_R \\ \Delta\theta \\ \Delta\varphi_e \end{pmatrix} = J \begin{pmatrix} \Delta\varphi_1 \\ \Delta\varphi_2 \\ \Delta\varphi_3 \\ \Delta\varphi_4 \end{pmatrix} \quad (20)$$

With these movements, the new pose in world frame $x_k = (x_k, y_k, \theta_k)^T$ can be calculated based on the pose before the movement (x_{k-1}):

$$\begin{aligned} x_k &= x_{k-1} + \Delta x_R \cos\left(\theta_{k-1} + \tfrac{\Delta\theta}{2}\right) \\ &\quad - \Delta y_R \sin\left(\theta_{k-1} + \tfrac{\Delta\theta}{2}\right) \\ y_k &= y_{k-1} + \Delta x_R \sin\left(\theta_{k-1} + \tfrac{\Delta\theta}{2}\right) \\ &\quad + \Delta y_R \cos\left(\theta_{k-1} + \tfrac{\Delta\theta}{2}\right) \\ \theta_k &= \theta_{k-1} + \Delta\theta \end{aligned} \quad (21)$$

A. Uncertainty Modeling

The movements of the vehicle are corrupted by noise caused by mechanical inaccuracies. Experiments with the omnidirectional vehicle show that the noise is mainly caused by slippage of the Mecanum wheels. Since the slippage of the wheels depends on the rotational speed of the free spinning rollers, the uncertainty depends on the direction of

the movement in vehicle frame. Therefore, it is assumed that the movements of the vehicle in vehicle frame are corrupted by independent noise ϵ_i:

$$\Delta \hat{x}_R = \Delta x_R + \epsilon_x \,, \ \Delta \hat{y}_R = \Delta y_R + \epsilon_y \,, \ \Delta \hat{\theta}_R = \Delta \theta_R + \epsilon_\theta \quad (22)$$

Furthermore, it is assumed that the noise ϵ_i is normally distributed with zero mean $\epsilon_i = \mathcal{N}(0, \sigma_i^2)$. The standard deviation σ_i is proportional to the displacement in the vehicle frame and changes in the coupling error $\Delta \varphi_e$:

$$\begin{pmatrix} \sigma_x \\ \sigma_y \\ \sigma_\theta \end{pmatrix} = \begin{pmatrix} \alpha_x^x & \alpha_x^y & \alpha_x^\theta & \alpha_x^e \\ \alpha_y^x & \alpha_y^y & \alpha_y^\theta & \alpha_y^e \\ \alpha_\theta^x & \alpha_\theta^y & \alpha_\theta^\theta & \alpha_\theta^e \end{pmatrix} \begin{pmatrix} \Delta x_R \\ \Delta y_R \\ \Delta \theta_R \\ \Delta \varphi_e \end{pmatrix} \quad (23)$$

The parameters α_i^j are vehicle-specific constants, which have to be identified by experiments.

With the additional noise, the motion model can be described as follows:

$$\boldsymbol{x}_k = \boldsymbol{f}(\boldsymbol{x}_{k-1}, \boldsymbol{u}_k, \boldsymbol{w}_k), \quad \text{with} \quad \boldsymbol{x}_k = \begin{pmatrix} x_k \\ y_k \\ \theta_k \end{pmatrix}, \quad (24)$$

$$\boldsymbol{u}_k = \begin{pmatrix} \Delta x_R \\ \Delta y_R \\ \Delta \theta_R \\ \Delta \varphi_e \end{pmatrix}, \quad \boldsymbol{w}_k = \begin{pmatrix} \epsilon_x \\ \epsilon_y \\ \epsilon_\theta \end{pmatrix}$$

$$\begin{aligned} x_k &= x_{k-1} + (\Delta x_R + \epsilon_x) \cos\left(\theta_{k-1} + \tfrac{\Delta\theta+\epsilon_\theta}{2}\right) \\ &\quad -(\Delta y_R + \epsilon_y) \sin\left(\theta_{k-1} + \tfrac{\Delta\theta+\epsilon_\theta}{2}\right) \\ y_k &= y_{k-1} + (\Delta x_R + \epsilon_x) \sin\left(\theta_{k-1} + \tfrac{\Delta\theta+\epsilon_\theta}{2}\right) \\ &\quad +(\Delta y_R + \epsilon_y) \cos\left(\theta_{k-1} + \tfrac{\Delta\theta+\epsilon_\theta}{2}\right) \\ \theta_k &= \theta_{k-1} + \Delta\theta + \epsilon_\theta \end{aligned} \quad (25)$$

B. Linearization

In order to use the motion model in an EKF, $\boldsymbol{f}(\bullet)$ has to be linearized. In the prediction step of the EKF, the estimated pose of the vehicle

$$\hat{\boldsymbol{x}}_k = \boldsymbol{f}(\hat{\boldsymbol{x}}_{k-1}, \boldsymbol{u}_k, \boldsymbol{0}) \quad (26)$$

and the covariance of the pose

$$\boldsymbol{P}_k = \boldsymbol{\Phi}_k \boldsymbol{P}_{k-1} \boldsymbol{\Phi}_k^T + \boldsymbol{W}_k \boldsymbol{Q}_k \boldsymbol{W}_k^T, \quad (27)$$

can be calculated based on $\boldsymbol{f}(\bullet)$ and its Jacobians $\boldsymbol{\Phi}_k$ and $\boldsymbol{W}_k$:

$$\boldsymbol{\Phi}_k = \frac{\partial \boldsymbol{f}}{\partial \boldsymbol{x}}(\hat{\boldsymbol{x}}_{k-1}, \boldsymbol{u}_k, \boldsymbol{0}) = \quad (28)$$

$$\begin{pmatrix} 1 & 0 & -\Delta x_R \sin\theta'_{k-1} - \Delta y_R \cos\theta'_{k-1} \\ 0 & 1 & \Delta x_R \cos\theta'_{k-1} - \Delta y_R \sin\theta'_{k-1} \\ 0 & 0 & 1 \end{pmatrix},$$

$$\text{with} \quad \theta' = \theta_{k-1} + \frac{\Delta\theta}{2}$$

$$\boldsymbol{W}_k = \frac{\partial \boldsymbol{f}}{\partial \boldsymbol{w}}(\hat{\boldsymbol{x}}_{k-1}, \boldsymbol{u}_k, \boldsymbol{0}) = \quad (29)$$

$$\begin{pmatrix} \cos\theta' & -\sin\theta' & -\tfrac{1}{2}\Delta x_R \sin\theta' - \tfrac{1}{2}\Delta y_R \cos\theta' \\ \sin\theta' & \cos\theta' & \tfrac{1}{2}\Delta x_R \cos\theta' - \tfrac{1}{2}\Delta y_R \sin\theta' \\ 0 & 0 & 1 \end{pmatrix}.$$

The process covariance matrix

$$\boldsymbol{Q}_k = \begin{pmatrix} \sigma_x^2 & 0 & 0 \\ 0 & \sigma_y^2 & 0 \\ 0 & 0 & \sigma_\theta^2 \end{pmatrix} \quad (30)$$

can be calculated using (23).

C. Motion Sampling Algorithm

Eqn. (25) can be used to develop the motion sampling algorithm, which is needed by the Monte Carlo localization procedure. Algorithm 1 shows the sequence of calculations to sample the particles.

Algorithm 1 Motion sampling algorithm

1: **sample_motion_model($\boldsymbol{x}_{k-1}, \boldsymbol{u}_k$)**

2: $\begin{pmatrix} \sigma_x \\ \sigma_y \\ \sigma_\theta \end{pmatrix} = \begin{pmatrix} \alpha_x^x & \alpha_x^y & \alpha_x^\theta & \alpha_x^e \\ \alpha_y^x & \alpha_y^y & \alpha_y^\theta & \alpha_y^e \\ \alpha_\theta^x & \alpha_\theta^y & \alpha_\theta^\theta & \alpha_\theta^e \end{pmatrix} \cdot \boldsymbol{u}_k$

3: $\Delta \hat{x}_R = \Delta x_R + \textbf{sample}(\sigma_x)$

4: $\Delta \hat{y}_R = \Delta y_R + \textbf{sample}(\sigma_y)$

5: $\Delta \hat{\theta} = \Delta\theta + \textbf{sample}(\sigma_\theta)$

6: $\hat{\theta}' = \theta_{k-1} + \Delta\hat{\theta}/2$

7: $x_k = x_{k-1} + \Delta\hat{x}_R \cos\hat{\theta}' - \Delta\hat{y}_R \sin\hat{\theta}'$

8: $y_k = y_{k-1} + \Delta\hat{y}_R \cos\hat{\theta}' + \Delta\hat{x}_R \sin\hat{\theta}'$

9: $\theta_k = \theta_{k-1} + \Delta\hat{\theta}$

10: **return** $\boldsymbol{x}_k = (x_k, y_k, \theta_k)^T$

VII. Experimental Results

We have made several experiments with one of our omnidirectional robots in our lab on the NaviFloor® installation. The measurements of the RFID reader and the wheel encoders are stored in a file and evaluated off-line with Matlab.

Fig. 6 shows comparative results of one experiment. The experimental data are the same as presented in [7] but evaluated with the extended algorithms presented in this paper. The robot moves a rectangle path $1.5\,\text{m} \times 3\,\text{m}$ in clockwise direction with constant heading ($\theta = 100°$). The path is transverse to the grid with an angle of 10°. The path starts and ends near tag position ($x = 1750\,\text{mm}$, $y = 4500\,\text{mm}$). All estimators are started after detecting the second tag (1750 mm, 4750 mm) (see Sec. IV-D). Hence, after global localization, the estimated heading is parallel to the grid ($\hat{\theta} = 90°$). Since odometry (magenta curve) is performed without measurement update, its position estimate differs much from real path (black curve). After detecting additional tags, all filters correct the estimated heading and therefore the direction of movement. The blue curve in Fig. 6 shows, that the PF needs the least way length to correct the misalignment. After detecting the fifth tag, both KFs corrects the pose estimate and follow the real path. The Quantized EKF with RSSI measurement (QRSSI, green curve) tends to force the position estimate into direction of the center of detected tags. The Constrained EKF with RSSI measurement (CRSSI, red cure) is able to follow the real path with a smaller deviation than the QRSSI. Table II compares the root mean square error (RMSE in mm) of the described filters with the estimators QEKF, CEKF, PF1000 presented in [7].
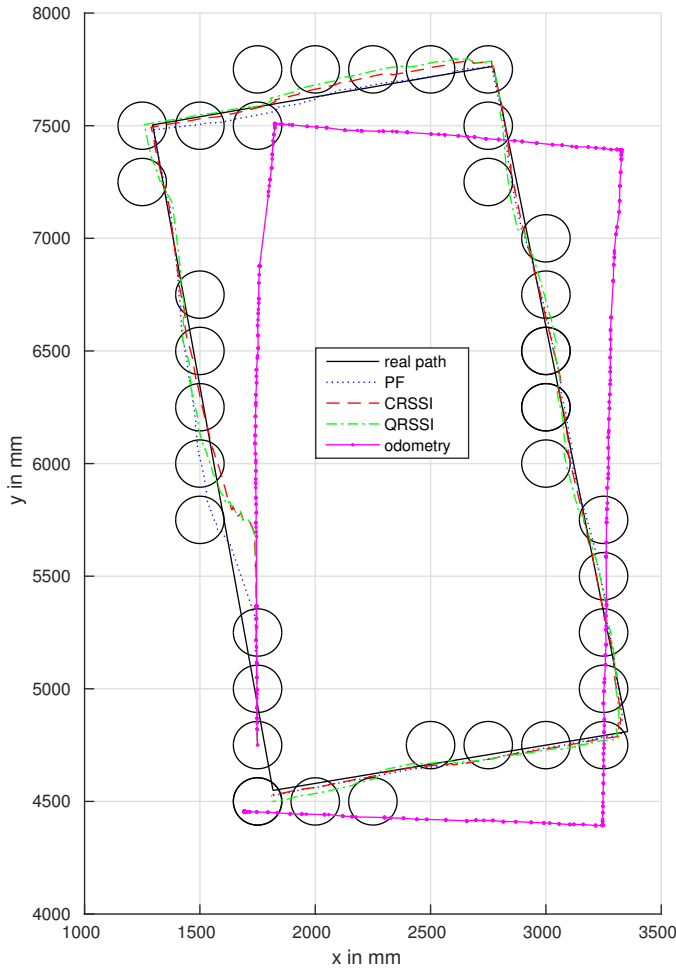
Fig. 6. Comparative results of one experiment

TABLE II
COMPARATIVE RESULTS OF PROPOSED ESTIMATORS

algorithm	QEKF	QRSSI	CEKF	CRSSI	PF1000	PFRSSI
RMSE	39.4	36.8	29.5	25.4	~ 30	~ 25
runtime	0.27	0.29	0.29	0.31	85.4	90.5

All estimators provide a better accuracy if the RSSI measurements are included in the algorithm. The accuracy of the proposed Constrained EKF is similar to a PF with high particle count (1000 particles). A PF with a low particle count (100 particles) has a much lower accuracy than both KF variants (see [7]). Owing to the particle sampling with random numbers, the RMSE for both PFs differ with every run. Further experiments confirm this accuracy of the evaluated filters. The CRSSI outperforms the QRSSI in most cases and provides a similar performance than a PF with high particle count.

Table II compares the duration for one motion plus measurement update of the filters in Milliseconds. The durations are measured with Matlab R2014b on a PC with Intel Core i7-2600 CPU 3.40 GHz. The measured durations show that a PF with high particle count is not able to run in real time even on a high speed PC. Fig. 7 shows the Cumulative Distribution Function (CDF) of th localization errors.
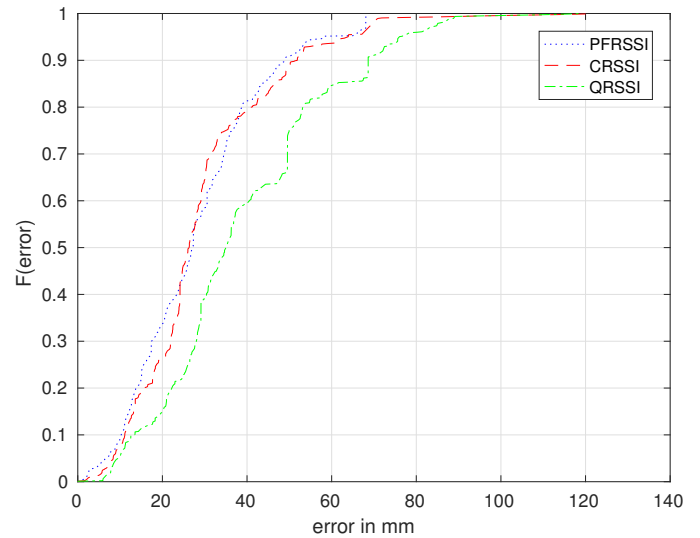

Fig. 7. Cumulative Distribution Function (CDF) of localization errors

VIII. CONCLUSIONS

In this paper, we have developed two localization algorithm based on Kalman filtering that fuses sensory data from wheel encoders with RFID RSSI measurements. The Quantized Kalman filter assumes RFID readings as quantized measurements of the robot position. The quantization noise depends on the RSSI of the RFID reading. The Constrained Kalman filter assumes the RFID readings as a noisy constraint of the robot's pose. This constraints depend on the RSSI of the RFID reading. The application of the proposed algorithms is possible for any RFID equipment which measures the RSSI from detected RFID tags. The localization accuracy of the Constrained EKF is similar to a PF but with much less computational expense. The accuracy of the Quantized EKF is slightly lower than the Constrained EKF. The accuracy of both localization methods is sufficient for most industrial applications.

The localization concept is suitable for small and inexpensive mobile robots, since the robots must be equipped with an inexpensive and small HF RFID reader only. The installation of the RFID infrastructure causes the highest expense for this localization method, but since passive RFID technology is used, the infrastructure is free of maintenance costs.

REFERENCES

[1] E. Guizzo, "Three Engineers, Hundreds of Robots, one Warehouse," *IEEE Spectrum*, vol. 7, pp. 27–34, 2008.
[2] G. Liu, W. Yu, and Y. Liu, "Resource management with RFID technology in automatic warehouse system," in *Intelligent Robots and Systems, 2006 IEEE/RSJ International Conference on*, 2006, pp. 3706–3711.
[3] T. Kämpke, B. Kluge, and M. Strobel, "Exploiting RFID capabilities onboard a service robot platform," in *Towards Service Robots for Everyday Environments*, ser. Springer Tracts in Advanced Robotics, E. Prassler, M. Zöllner, R. Bischoff, W. Burgard, R. Haschke, M. Hägele, G. Lawitzky, B. Nebel, P. Plöger, and U. Reiser, Eds. Springer Berlin Heidelberg, 2012, vol. 76, pp. 215–225.
[4] Götting KG, "Introduction transponder positioning," http://www.goetting-agv.com/components/transponder/introduction.
[5] M. Baum, B. Niemann, and L. Overmeyer, "Passive 13.56 MHz RFID transponders for vehicle navigation and lane guidance," in *Proceedings of the 1st International EUR AS IP Workshop on RFID Technology*, 2007, pp. 83–86.

[6] C. Röhrig, A. Heller, D. Heß, and F. Künemund, "Global localization and position tracking of automatic guided vehicles using passive RFID technology," in *Proceedings of the joint 45th International Symposium on Robotics (ISR 2014) and the 8th German Conference on Robotics (ROBOTIK2014)*, Munich, Germany, Jun. 2014.

[7] C. Röhrig, D. Heß, and F. Künemund, "Constrained Kalman filtering for indoor localization of transport vehicles using floor-installed HF RFID transponders," in *Proceedings of the 9th Annual IEEE International Conference on RFID (IEEE RFID 2015)*, San Diego, CA USA, Apr. 2015, pp. 113–120.

[8] C. Röhrig, Heß, and F. Künemund, "Global localization of mobile robots using signal strength readings from floor-installed rfid transponders," in *Lecture Notes in Engineering and Computer Science: Proceedings of The International MultiConference of Engineers and Computer Scientists 2016, IMECS 2016*, Hong Kong, 16-18 March, 2016, pp. 179–184.

[9] K. Kodaka, H. Niwa, Y. Sakamoto, M. Otake, Y. Kanemori, and S. Sugano, "Pose estimation of a mobile robot on a lattice of RFID tags," in *Intelligent Robots and Systems, 2008. IROS 2008. IEEE/RSJ International Conference on*, 2008, pp. 1385–1390.

[10] J. Mi and Y. Takahashi, "Performance analysis of mobile robot self-localization based on different configurations of rfid system," in *Proceedings of the 2015 IEEE International Conference on Advanced Intelligent Mechatronics (AIM)*. IEEE, July 2015, pp. 1591–1596.

[11] ——, "Low cost design of hf-band rfid system for mobile robot self-localization based on multiple readers and tags," in *Proceedings of the 2015 IEEE International Conference on Robotics and Biomimetics (ROBIO)*. IEEE, Dec 2015, pp. 194–199.

[12] B.-S. Choi, J.-W. Lee, J.-J. Lee, and K.-T. Park, "A hierarchical algorithm for indoor mobile robot localization using RFID sensor fusion," *Industrial Electronics, IEEE Transactions on*, vol. 58, no. 6, pp. 2226–2235, 2011.

[13] J. Lee, Y. Park, D. Kim, M. Choi, T. Goh, and S.-W. Kim, "An efficient localization method using RFID tag floor localization and dead reckoning," in *Control, Automation and Systems (ICCAS), 2012 12th International Conference on*, 2012, pp. 1452–1456.

[14] E. DiGiampaolo and F. Martinelli, "A passive UHF-RFID system for the localization of an indoor autonomous vehicle," *Industrial Electronics, IEEE Transactions on*, vol. 59, no. 10, pp. 3961–3970, 2012.

[15] M. Boccadoro, F. Martinelli, and S. Pagnottelli, "Constrained and quantized kalman filtering for an RFID robot localization problem," *Autonomous Robots*, vol. 29, no. 3-4, pp. 235–251, 2010.

[16] A. Levratti, M. Bonaiuti, C. Secchi, and C. Fantuzzi, "An inertial/RFID based localization method for autonomous lawnmowers," in *Proceedings of the 10th IFAC Symposium on Robot Control, IFAC SYROCO 2012*, Dubrovnik, Croatia, Sep. 2012, pp. 145–150.

[17] M. Ahmad and A. Mohan, "Novel bridge-loop reader for positioning with HF RFID under sparse tag grid," *Industrial Electronics, IEEE Transactions on*, vol. 61, no. 1, pp. 555–566, 2014.

[18] T. Kämpke, B. Kluge, E. Prassler, and M. Strobel, "Robot position estimation on a RFID-tagged smart floor," in *Field and Service Robotics*, ser. Springer Tracts in Advanced Robotics, C. Laugier and R. Siegwart, Eds. Springer Berlin Heidelberg, 2008, vol. 42, pp. 201–211.

[19] K. Kodaka and S. Sugano, "Reader antennas' configuration effects for two wheeled robots on floor-installed RFID infrastructure – analysis of forward-backward configuration effect," in *Intelligent Robots and Systems (IROS), 2010 IEEE/RSJ International Conference on*, 2010, pp. 5718–5724.

[20] S. Kim and H. Kim, "Pseudorandom tag arrangement for accurate RFID based mobile robot localization," in *Advanced Radio Frequency Identification Design and Applications*, S. Preradovic, Ed. InTech, 2011.

[21] S. Han, J. Kim, C.-H. Park, H.-C. Yoon, and J. Heo, "Optimal detection range of RFID tag for RFID-based positioning system using the k-nn algorithm," *Sensors*, vol. 9, no. 6, pp. 4543–4558, 2009.

[22] R. E. Curry, *Estimation and Control with Quantized Measurements*. MIT Press Cambridge, 1970.

[23] D. Simon, "Kalman filtering with state constraints: a survey of linear and nonlinear algorithms," *Control Theory Applications, IET*, vol. 4, no. 8, pp. 1303–1318, August 2010.

[24] V. Sircoulomb, G. Hoblos, H. Chafouk, and J. Ragot, "State estimation under nonlinear state inequality constraints. a tracking application,"

in *Control and Automation, 2008 16th Mediterranean Conference on*, June 2008, pp. 1669–1674.

[25] A. Steinhage and C. Lauterbach, "SensFloor® and NaviFloor®: Large-area sensor systems beneath your feet," in *Handbook of Research on Ambient Intelligence and Smart Environments: Trends and Perspectives*, N. Chong and F. Mastrogiovanni, Eds. Hershey, PA: Information Science Reference, 2011, pp. 41–55.

[26] C. Röhrig, D. Heß, C. Kirsch, and F. Künemund, "Localization of an Omnidirectional Transport Robot Using IEEE 802.15.4a Ranging and Laser Range Finder," in *Proceedings of the 2010 IEEE/RSJ International Conference on Intelligent Robots and Systems (IROS 2010)*, Taipei, Taiwan, Oct. 2010, pp. 3798–3803.

[27] D. Heß, F. Künemund, and C. Röhrig, "Linux based control framework for mecanum based omnidirectional automated guided vehicles," in *Lecture Notes in Engineering and Computer Science: Proceedings of The World Congress on Engineering and Computer Science 2013, WCECS 2013*, San Francisco, USA, 23-25 October, 2013, pp. 395–400.

[28] P. F. Muir, "Modeling and Control of Wheeled Mobile Robots," Ph.D. dissertation, Carnegie Mellon University, 1988.

[29] D. Heß, F. Künemund, and Röhrig, "Simultaneous calibration of odometry and external sensors of omnidirectional automated guided vehicles (AGVs)," in *Proceedings of the 47th International Symposium on Robotics (ISR 2016)*, Munich, Germany, Jun. 2016, pp. 480–487.

Christof Röhrig received his Diploma degree from the University of Bochum, Germany, in 1993, and his Doctor degree from the University of Hagen, Germany, in 2003, both in electrical engineering. Between 1993 and 1997 he was head of Automated Systems Engineering at Reinoldus Transport- und Robotertechnik GmbH Dortmund, Germany. From 1997 until 2003 he was with the Control Systems Engineering Group at University of Hagen. Since 2003, he is Professor of Computer Science at the University of Applied Sciences and Arts in Dortmund, Germany, where he heads the Intelligent Mobile Systems Lab. His current research interests include mobile robots and localization using wireless technologies.

Daniel Heß received his Diploma degree in 2008, and the Masters degree in 2010, both in computer science from the University of Applied Sciences and Arts in Dortmund, Germany. Since 2008, he is working in different research projects at the Intelligent Mobile Systems Lab, University of Applied Sciences and Arts Dortmund, where he is currently working toward the Doctor degree. His current research interests include sensor data fusion and localization.

Frank Künemund received his Diploma degree in 2008, and the Masters degree in 2010, both in computer science from the University of Applied Sciences and Arts in Dortmund, Germany. Since 2008, he is working in different research projects at the Intelligent Mobile Systems Lab, University of Applied Sciences and Arts in Dortmund, where he is currently working toward the Doctor degree. His current research interests include path planning for omnidirectional mobile robots.